Original Research

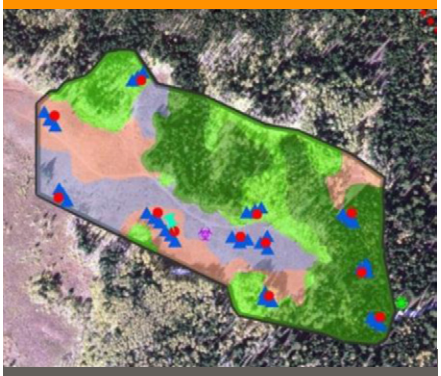

Cosmic-ray neutron probe (CRNP) soil moisture estimates were compared with measurements from a soil moisture sensor network revealing that near-surface numerically simulated estimates improved correlation. Additional calibration during the wet period significantly improved CRNP correlations over traditional one-time calibration taken under drier conditions.

Measured and Modeled Soil Moisture Compared with Cosmic-Ray Neutron Probe Estimates in a Mixed Forest

Ling Lv, Trenton E. Franz, David A. Robinson, and Scott B. Jones*

Soil moisture is a key variable in most environmental processes, and the cosmic-ray neutron probe (CRNP) fills a niche for intermediate-scale soil moisture measurements. In this study, the CRNP estimated soil moisture was compared with a soil moisture measurement network including 108 time domain transmissometry (TDT) probes. We also used a Hydrus-1D numerical model of measured soil moisture at targeted locations by inversely fitting soil hydraulic parameters used to simulate soil moisture in the near surface (0.03 and 0.05 m) during the growing seasons of 2011 and 2012. Both simulated and TDT-measured soil moisture were used in constructing the depth-weighted mean areal soil moisture for comparison with the CRNP estimates. The results showed that near-surface soil moisture estimated by the numerical simulation improved the correlation between the sensor network and the CRNP estimation, especially during rainfall events. The CRNP estimates of soil moisture exhibited a dry bias under relatively wet conditions at the beginning of the snow-free period because of the almost binary spatial distribution of soil moisture. Using a combination of soil moisture measurements and near-surface simulations, the CRNP output was recalibrated to capture the wetter conditions, resulting in a RMSE (0.011 m^3/m^3) of less than half the original calibration RMSE (0.025 m^3/m^3). The calibration was validated using CRNP data from the 2013 growing season against independent soil moisture values.

Abbreviations: COSMOS, Cosmic-ray Soil Moisture Observing System; CRNP, cosmic-ray neutron probe; EC_a, apparent electrical conductivity; RMSE, root mean square error; RSM, response surface methodology; TDR, time domain reflectometry; TDT, time domain transmissometry; TWDEF, T.W. Daniel Experimental Forest.

L. Lv and S.B. Jones, Dep. of Plants, Soils and Climate, Utah State Univ., 4820 Old Main Hill, Logan, UT 84322-4820; T.E. Franz, School of Natural Resources, Univ. of Nebraska, 607 Hardin Hall, Lincoln, NE 68583; and D.A. Robinson, NERC-Centre for Ecology and Hydrology, Environment Centre Wales, Deiniol Rd., Bangor Gwynedd, LL57 2UW, UK. *Corresponding author (scott.jones@usu.edu).

Vadose Zone J.
doi:10.2136/vzj2014.06.0077
Received 27 June 2014.
Accepted 2 Nov. 2014.

Soil moisture is an important variable impacting most ecological and environmental processes. It significantly affects the ongoing exchange of water and energy between the land and atmosphere (Wang et al., 2005; Seneviratne et al., 2010). Antecedent soil moisture governs the generation of runoff and resulting flooding due to its effect on infiltration capacities (Minet et al., 2011). Reliable simulations of these processes require areal averages of soil moisture measured at intermediate or larger scales (Ochsner et al., 2013; Robinson et al., 2008). Therefore, the compatibility of soil moisture model and measurement scales dictates the quality of the resulting simulations (Scipal et al., 2005). The degree of soil moisture variability not only depends on static factors such as soil texture, soil organic matter, soil structure. etc., but also on dynamic factors such as vegetation, weather conditions, etc. (Crow et al., 2012; Reynolds, 1970). Due to greater variation in topography and vegetation cover, nonuniform litter input, and less soil mixing (i.e., as opposed to bioturbation), the soil moisture distribution in a natural ecosystem often exhibits more heterogeneity than cropland (Flinn and Marks, 2007; Hawley et al., 1983), requiring a larger sampling size. Regarding the scale of soil moisture determination, the point scale has made major advances, with a broad selection of precise, affordable, in situ sensors now available (Blonquist et al., 2005a; Bogena et al., 2007; Jones et al., 2005; Robinson et al., 2003a; Rosenbaum et al., 2010; Vereecken

et al., 2008), while at larger remote-sensing scales, capabilities continue to improve, although presently with less accuracy at regional and continental scales. A glaring intermediate-scale gap for soil moisture assessment remains (Ochsner et al., 2013; Robinson et al., 2008), but the development of the cosmic-ray neutron probe (CRNP, Hydroinnova) offers the ability to assess scales of hundreds of meters.

The CRNP is a novel, non-invasive technique (Shuttleworth et al., 2010) to measure the areal-averaged soil moisture of an effective depth on the order of decimeters within a radial footprint on the order of several hundred meters (Zreda et al., 2008, 2012). This technique is analogous to the neutron probe used for downhole soil moisture measurements (Kramer et al., 1992), but the equilibrium intensity of fast neutrons are measured by the CRNP instead of thermalized neutrons as with the downhole method. This causes the response to be inversely instead of directly correlated. It is known that secondary cosmic rays interact with the nuclei of atoms in the atmosphere, water, vegetation, and soil, leading to the emission of fast neutrons in the atmosphere, and those fast neutrons are mainly moderated by H atoms (Zreda et al., 2011). Franz et al. (2012) suggested that the CRNP is highly sensitive to the shallow subsurface soil moisture, but a lack of shallow (<0.1-m) soil moisture measurements limited their conclusions in this regard. The radial footprint of the CRNP is a surface diameter of about 600 m at sea level in dry air, but that sensing diameter increases with increasing elevation and decreases with increasing atmospheric humidity (Desilets and Zreda, 2013).

The objectives of this research were to compare the growing season CRNP soil moisture estimates in a mixed forest using a horizontal and depth-weighted averaging approach with (i) measurements from a network of 108 time domain transmissometry (TDT) soil moisture sensors and (ii) 36 numerically simulated soil water content profiles.

Theoretical Considerations

The CRNP measures moderated neutron counts and records totals every hour. The plastic shielding around the CRNP detector tube moderates the incoming fast neutrons so that they are detected principally as epithermal neutrons, with only 30% being detected as thermal neutrons (for further discussion, see McJannet et al., 2014). Using a neutron particle transport model, Desilets et al. (2010) found a theoretical relationship between relative neutron counts and soil moisture in homogeneous sand (SiO_2):

$$\theta_g(N) = \frac{a_0}{N/N_0 - a_1} - a_2 \qquad [1]$$

where $\theta_g(N)$ (g/g) is the average gravimetric soil moisture, and empirical fitting parameters are given by $a_0 = 0.0808$, $a_1 = 0.372$, and $a_2 = 0.115$. The neutron counting rate, N, is the output from the CRNP in counts per hour, which are the quality-controlled data corrected to account for temporal changes in pressure and incoming neutron flux and then rescaled to match the location and configuration of the CRNP located in the San Pedro River basin in Arizona. For more information on the quality-control and correction procedures, see Zreda et al. (2008, 2012). The neutron counting rate, N, is presented on the website of the national Cosmic-ray Soil Moisture Observing System (COSMOS) under Data Level 2 (http://cosmos.hwr.arizona.edu/). In addition, a water vapor correction factor following Rosolem et al. (2013) was used to further reduce noise in the neutron intensity. We note that the COSMOS website does not correct for changes in water vapor at this time in Level 2 data because not all sites have readily available meteorological information to compute the correction factor in real time. The variable N_0 is the neutron counting rate over dry soil under the same reference conditions and needs to be estimated with at least one independent soil moisture calibration.

In non-agricultural ecosystems, the hourly neutron counting rate in Eq. [1] is influenced not only by soil moisture but also by H in other water-related sources, which include soil lattice water, soil organic matter, atmospheric water vapor, and water in or on vegetation. Previous research (Zreda et al., 2012) suggested a methodology to correct for lattice water and H in soil organic matter by partitioning them from the total moisture and correcting for atmospheric water vapor by assigning a correction factor to the hourly neutron counting rate:

$$N' \quad NC_{WV} \qquad [2]$$

where N' is the water vapor corrected neutron count rate (counts/h) and C_{WV} is the atmospheric water vapor correction factor (Rosolem et al., 2013), determined as

$$C_{WV} = 1 + 0.0054\left(\rho_v - \rho_v^{ref}\right) \qquad [3]$$

where ρ_v is the measured absolute water vapor (g/m^3) and ρ_v^{ref} is the absolute water vapor (g/m^3) at a reference condition (in this study we used dry air, $\rho_v^{ref} = 0$ g/m^3).

Finally, the soil moisture, θ_v (m^3/m^3), is determined as

$$\theta_v = \left[\frac{a_0}{N'/N_0' - a_1} - a_2 - (\rho_{SOM} + \rho_\tau)\right]\rho_b \qquad [4]$$

where ρ_τ is the weight fraction of lattice water in dry soil (g/g), ρ_{SOM} is the weight fraction of soil organic matter water equivalent in dry soil (g/g), ρ_b is soil bulk density (g/cm^3), and N_0' is the atmospheric water vapor corrected value of N_0.

In the subsurface, we assume that the CRNP measurement support volume is a cylinder with a depth that varies with soil pore water (θ_v, m^3/m^3), lattice water (ρ_τ, g/g), soil organic matter (ρ_{SOM}, g/g), and soil bulk density (ρ_b, g/cm^3). Franz et al. (2013) calculated the effective depth, $z^*(\theta_v)$ (m), using

$$z^*(\theta_v) = \frac{0.058}{\rho_b(\rho_\tau + \rho_{SOM}) + \theta_v + 0.0829} \qquad [5]$$

Materials and Methods

Study Area

The study area lies within the Utah State University T.W. Daniel Experimental Forest (TWDEF), located approximately 30 km northeast of Logan, UT (41.86° N, 111.50° W; Fig. 1). The climate is typical of the montane semiarid Intermountain West, with a mid-growing-season (July) mean temperature of 14.4°C and mean precipitation of 950 mm/yr, 80% of which falls as snow. Snowmelt typically occurs between mid-May and mid-June. The mean growing season occurs between May and September, when mean rainfall totals are 277 mm, with July and August typically getting <20 mm (Van Miegroet et al., 2005). The site is a gently sloping (<10%) northeast- to southeast-trending ridgetop at the head of a contributing watershed to the Logan River and Bear River basins. The study site has an area of 86,000 m^2 and an elevation around 2600 m. The soil formed in aeolian deposits overlying residuum and colluvium from the Wasatch formation (Woldeselassie et al., 2012). The forest soils (aspen and conifer) were classified as fine to coarse-loamy to loamy-skeletal Haplocryalfs, and the rangeland soils (sagebrush and grass) were classified as fine-loamy to loamy-skeletal Haploxeralfs (Olsen and Van Miegroet, 2010). Additionally, the conifer forest soil had characteristic O horizons (<0.03 m), and aspen forest and non-forest soils lacked an O horizon (Olsen and Van Miegroet, 2010).

The landscape is a patchwork of four dominant vegetation communities common to the Intermountain region. Forest communities include aspen (*Populus tremuloides* Michx.) and conifer, predominantly Engelmann spruce (*Picea engelmannii* Parry ex Engelm.) and subalpine fir [*Abies lasiocarpa* (Hook.) Nutt.]. The tree size

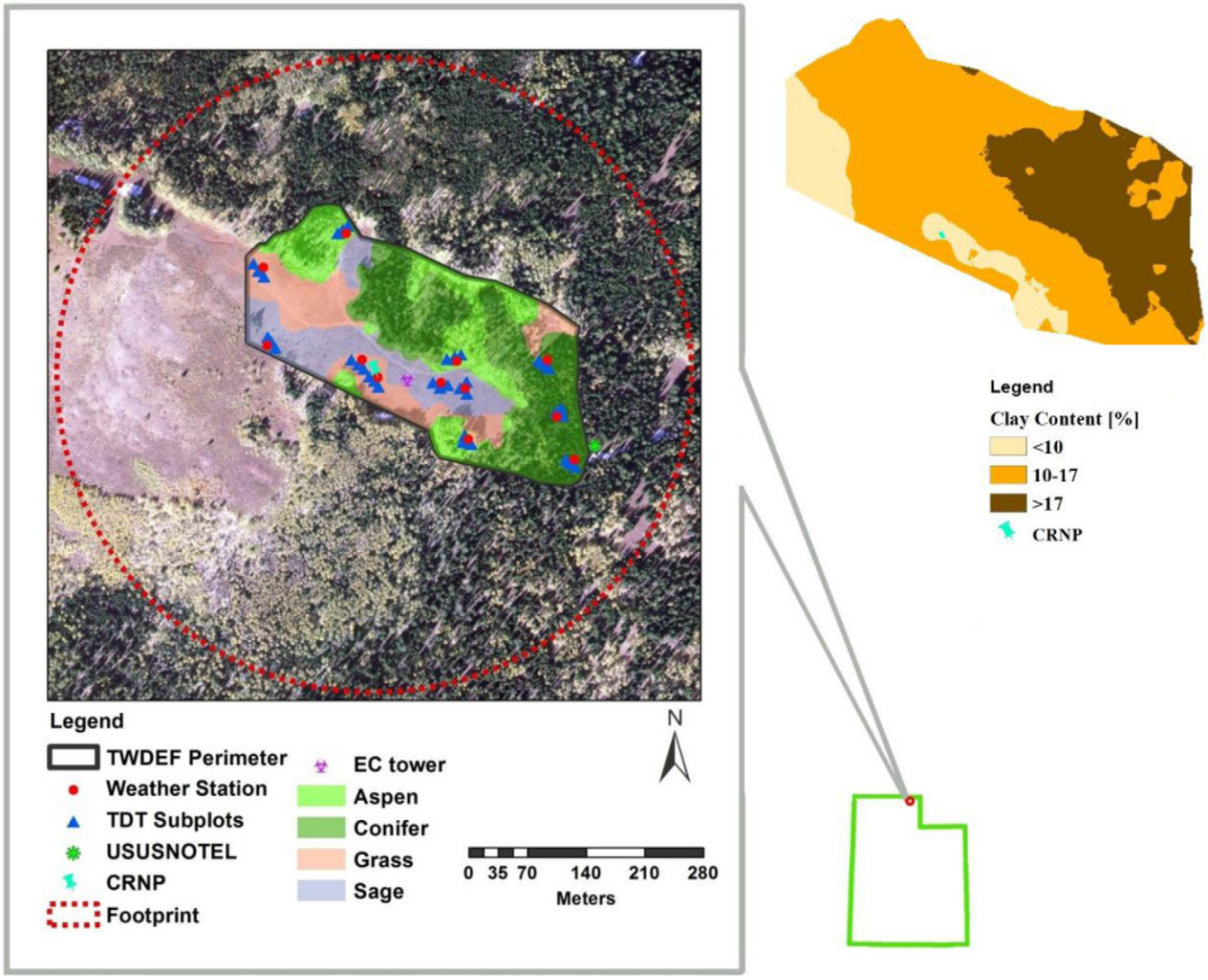

Fig. 1. The overview of the T.W. Daniel Experimental Forest (TWDEF) study site in northern Utah and the layout of the data collection network contained within the fenced perimeter. A cosmic-ray neutron probe (CRNP) and its associated footprint are also shown. The time domain transmissometry (TDT) soil moisture sensors are shown as triangles around each plot weather station. Utah State University's Doc Daniel SNOTEL site (USUSNOTEL) is located at the eastern edge of the TWDEF enclosure. The clay content (%) distribution inside the TWDEF site is displayed in the upper right corner. Note the similarities in vegetation and clay content distribution.

distribution in the site is shown in Table 1. The dry aboveground biomass is 5.56 and 5.92 kg/m^2 for the aspen and the communities, respectively. Non-forest communities include grasses and forbs [dominated by *Bromus carinatus* Hook. & Arn. and *Elymus trachycaulus* (Link) Gould ex Shinners] and sagebrush (*Artemisia tridentate* Nutt.) (McArthur, 1983; Olsen and Van Miegroet, 2010). The distribution of these vegetation communities within the TWDEF site are: 21% aspen, 43% conifer, 18% grass, and 18% sagebrush. The distribution of aspen, conifer, grass, and sagebrush within the CRNP footprint are 33, 47, and 9, and 11%, respectively. All vegetation communities are characterized by similar elevation, aspect, climate, geomorphology, and geology (Van Miegroet et al., 2005).

Time-Domain Transmissometry Soil Moisture Sensor Network

Time-domain transmissometry sensors (Acclima, Inc.) provided travel-time measurements of dielectric permittivity to estimate the soil moisture, with soil temperature and electrical conductivity measurements also provided. The TDT operation principles can be found elsewhere (Jones et al., 2005; Robinson et al., 2003a), and its calibration to moisture relies on the method of Topp et al. (1980). The TDT method offers the advantage of having the pulse generating and sampling electronics mounted in the head of the probe, which allows TDT to be used with longer cable lengths and without the need for coaxial multiplexers, relying instead on sensor addressing and SDI-12 communications. The most important benefits are that TDT has developed as a low cost, small size, high stability and accurate method for measuring permittivity (Blonquist et al., 2005b). Direct comparisons of permittivity measurement accuracy using both TDT and time domain reflectometry (TDR) were made previously (Blonquist et al., 2005a; Schwartz et al., 2014; Topp et al., 2001). In our study site, three plots (Fig. 1) for each of the four dominant vegetation types were randomly selected and three subplots (5 by 5 m) within each plot were set up for statistical measurements. Within each subplot, TDT sensors were installed horizontally at depths of 0.10, 0.25, and 0.50 m, beginning measurements in September 2008. The TDT data were recorded with commercial dataloggers (CR1000/CR10X dataloggers, Campbell Scientific), and data were relayed via telemetry every 30 min to a data storage computer at Utah State University.

Table 1. Tree size distribution and characteristics determined from seven 100-m^2 plots at the T.W. Daniel Experimental Forest research site, the estimated aboveground biomass (AGB) following Jenkins et al. (2003), and the root biomass (RB) found within the top 0.3 m of the soil surface.

Mean stem diameter	Tree height	Stem density	Ratio of RB to AGB	Ratio of RB above 0.3 m to total RB	Dry AGB	Dry RB above 0.3 m
m		no./ha	%		kg/m^2	
Aspen						
0.025	4.83	24	25.5	40	0.002	0.0002
0.075	7.16	33	20.5	40	0.04	0.004
0.125	9.48	33	19.6	40	0.15	0.01
0.175	11.81	61	19.3	40	0.62	0.05
0.225	14.13	66	19.1	40	1.22	0.09
0.275	16.46	24	18.9	40	0.72	0.05
0.325	18.78	24	18.9	40	1.07	0.08
0.375	21.11	9	18.8	40	0.56	0.04
0.425	23.43	14	18.8	40	1.18	0.09
Total					5.56	0.41
Conifer						
0.025	7.38	67	27.3	40	0.01	0.0008
0.075	9.11	34	22.9	40	0.05	0.004
0.125	10.84	74	22.1	40	0.34	0.03
0.175	12.57	60	21.7	40	0.60	0.05
0.225	14.30	54	21.5	40	0.96	0.08
0.275	16.04	27	21.4	40	0.77	0.07
0.325	17.77	13	21.4	40	0.55	0.05
0.375	19.50	13	21.3	40	0.76	0.07
0.425	21.23	7	21.3	40	0.55	0.05
0.475	22.96	13	21.2	40	1.33	0.11
Total					5.92	0.51

Portable Time Domain Reflectometry Soil Moisture Measurements

The portable TDR consists of several components: a TDR100 time domain reflectometer (Campbell Scientific), a CR1000 datalogger, a two-rod steel TDR probe with 0.1-m length, an light-emitting diode (LED) display screen with control button, and a 12-V battery. We first calibrated the portable TDR probe length in water and in air (Robinson et al., 2003b) and subsequently used it to measure the soil moisture within the TWDEF site. Soil moisture was measured along five transects (directed north, northeast, northwest, west, and east, beginning near the CRNP and ending at the perimeter fence of the TWDEF site) by inserting the probe vertically into the soil (0–0.1 m). The spacing between measurements along each transect was 0.5 m. The TDR-based soil moisture measurement campaigns were implemented during the growing season of 2012. The first field campaign took place after snowmelt (7 June 2012), when the soil was expected to be wettest. Thereafter, the soil moisture was measured monthly, on 6 July, 1 Aug., and 2 Sept. 2012. These TDR sampling events recorded the soil moisture status under relatively wet, medium, and dry conditions. A CR1000 datalogger recorded volumetric soil moisture and the corresponding GPS location during sampling. The TDR data from different sampling dates were separated to analyze the structure of seasonal spatial variation in soil moisture using variograms. The analysis was done using Matlab 7.12 (R2011a) software and the implemented geostatistical functions *variogram* and *variogramfit*. The exponential model was chosen to fit to the experimental variograms.

Soil Texture Mapping

Following the method of Abdu et al. (2008), georeferenced apparent electrical conductivity (EC_a) measurements were taken non-invasively using a DUALEM-1S ground conductivity instrument coupled with a Trimble ProXT GPS unit. Electrical sensors are particularly suited to soil measurements because the EC_a of soil is highly dependent on the clay content, soil solution, and water content (Friedman, 2005). The electromagnetic induction (EMI) instrument was held approximately 0.4 m above the ground while traversing the instrumented area, resulting in an approximate penetration depth of 0.6 m and measurement volume of about 0.6 m^3. The EC_a data were acquired using a handheld GIS (HGIS, StarPal Inc.) program within an Allegro CX handheld field computer (Juniper Systems). The EMI mapping process required a few hours, with the EC_a data being collected every second. The EC_a data were subsequently checked for continuity and anomalous values using a time-series view of the data. Repeat and anomalous values (6.6% of the total), which can be caused by pauses in the survey or by buried metal fragments, wires, pipes, etc., were identified and removed from the data set as a quality control measure.

The EMI data were subsequently corrected and analyzed using geostatistical analysis techniques (Abdu et al., 2008), including normal score transformation and kriging. The spatial site selection algorithm in the ESAP software package (Lesch et al., 2000) was used to pick out 12 calibration sites where the soil was sampled for subsequent laboratory analysis of soil texture and EC. The selection algorithm, which uses response surface methodology (RSM), was developed by Lesch et al. (1995) to predict field-scale soil salinity from EC_a survey data using multiple linear regression models and a limited quantity of calibration samples. We adopted the site-selection technique to predict field-scale clay concentration due to the high correlation between soil textural properties and EC_a in low soil solution electrical conductivity soils such as those found in our study site.

Cosmic-Ray Neutron Probe Calibration

The CRNP probe (CRS 1000, Hydroinnova) was first installed at the TWDEF on 13 Aug. 2011 as part of the COSMOS system (Zreda et al., 2012). Calibration was performed on the same day, during which soil samples were collected at 18 locations along six compass transects (north, northeast, southeast, south, southwest, and northwest) at radial distances from the CRNP probe of 25, 75, and 200 m. Samples were collected at each location at six depths of 0 to 0.05, 0.05 to 0.1, 0.1 to 0.15, 0.15 to 0.2, 0.2 to 0.25, and 0.25 to 0.3 m for a total of 108 soil samples. For each sample, the soil water content and bulk density were determined by oven drying at 105°C. Soil lattice water and soil organic matter (SOM) content measurements in 1-g subsamples were taken from each of the 108 calibration samples. The 108-g aggregate sample was sent to Actlabs (http://www.actlabs.com) to measure the lattice water and SOM. The mean count reading from the CRNP between 16:00 and 22:00 h on 13 August was 1352 ± 20 counts/h and the mean absolute water vapor density was 6 g/m^3 (Table 2). With the installation date of the CRNP in August 2011, our study period was focused on the growing seasons of 2011 and 2012, with 2013 used as a validation year.

Numerical Model Simulation of Near-Surface Soil Moisture

Franz et al. (2012) suggested that the CRNP is highly sensitive to shallow subsurface soil moisture, but the lack of soil moisture measurements down to 0.1 m limited their conclusions regarding near-surface correlation at their study site in southern Arizona. Soil water content dynamics above 0.1 m were simulated using Hydrus-1D numerical simulation software, which is a soil process modeling software package (Šimůnek et al., 2008). The code combines a root water uptake model, the Penman–Monteith equation, and the Richards equation (Šimůnek et al., 2008) to simulate the soil water contents within the soil profile including the near surface for each subplot (36 subplots total). The vegetation types were represented in the Hydrus-1D model by the following parameters: (i) Feddes' parameters defining root water uptake reduction coefficients (Feddes et al., 1974, 2001)—the parameters we used are listed in Table 3; (ii) the albedo and extinction coefficient of each vegetation type; (iii) vegetation physiological stages represented by the leaf area index (LAI)—the LAI for conifer was assumed to be constant and was measured using a line quantum meter (MQ-301, Apogee), while the time dependence of the LAI of aspen, grass, and sagebrush during the growing season were modeled using a logistic growth function (Yu et al., 2010); and (iv) rooting depths determined based on soil surveys at the TWDEF site. The surveys found vegetation rooting depths down to 1.2 m with no groundwater found within their 2-m sampling depth. Therefore, we set the Hydrus-1D domain to be a 2-m vertical column with a numerical modeling grid resolution of 0.01 m. The soil profile was further divided into three layers according to the soil genetic horizon samples (Boettinger et al., 2004) for each plot and ensuring that each

Table 2. Summary of measured and derived parameters used in the calibration function (Eq. [4]) established 11 Aug. 2011 at the T.W. Daniel Experimental Forest.

Parameter	Value
Soil bulk density (ρ_b), g/cm^3	0.93
Weighted soil moisture on the calibration day (θ_v), m^3/m^3	0.134
Effective depth on the calibration day [$z^*(\theta_v)$], m	0.23
Weight fraction of soil organic matter water equivalent in dry soil (ρ_{SOM}), g/g	0.017
Weight fraction of lattice water in dry soil(ρ_T), g/g	0.028
Water vapor density on the calibration day (ρ_v), g/m^3	6
Neutron count on the calibration day (N), counts/h	1352
Site-specific constant (N_0'), counts/h	2189

Table 3. Feddes' parameters defining the root water uptake reduction coefficient, $\alpha(h)$, including the pressure head below which roots start to extract water from the soil (h_1), the pressure head below which roots extract water at the maximum possible rate (h_2), the limiting pressure head below which roots cannot longer extract water at the maximum rate (assuming a potential transpiration rate of T_{Phigh}) (h_{3h}), the limiting pressure head below which roots cannot longer extract water at the maximum rate (assuming a potential transpiration rate of T_{Plow}) (h_{3l}), the pressure head below which root water uptake ceases (usually taken at the wilting point) (h_4), and the high and low potential transpiration rates (T_{Phigh} and T_{Plow}, respectively) for the studied vegetation types (Havranek and Benecke, 1978; Kelliher et al., 1993; Kolb and Sperry, 1999; Running, 1976; Ryel et al., 2002, 2010; Taylor and Ashcroft, 1972).

Vegetation	h_1	h_2	h_{3h}	h_{3l}	h_4	T_{Phigh}	T_{Plow}
	m					m/d	
Aspen	0	0	−3.30	−20.00	−150.00	0.005	0.001
Conifer	0	0	−51.00	−128.00	−215.00	0.005	0.001
Grass/forbs	0	0	−3.00	−10.00	−150.00	0.005	0.001
Sagebrush	0	0	−4.00	−51.00	−330.00	0.0095	0.001

layer included a soil moisture sensor. The O horizon was not a dominant layer in the TWDEF site; for example, the conifer forest soil had a characteristic O horizon <0.03 m and aspen and the non-forest soils lacked an O horizon. Therefore, an O horizon was not included in the Hydrus-1D modeling as a simulation layer. Due to the lack of soil moisture sensor installation within the top 0.1 m, we used soil water content measured at the 0.1-, 0.25-, and 0.5-m depth as inputs to inversely solve for soil hydraulic parameters at each location and, using these soil hydraulic parameters, simulated the soil moisture at the 0.03- and 0.05-m depths during the growing seasons of 2011 and 2012. The lower boundary condition was set as a free-drainage boundary. The upper boundary condition was an atmospheric boundary condition, with surface runoff possible when excess water built up on the surface. The meteorological measurements were monitored at each automated micrometeorological tower (ATMs) (dots in Fig. 1) and used to compute the upper boundary condition. The ATMs provided measurements every 30 min for air temperature, air vapor pressure, wind speed, net radiation, and snow depth or summertime precipitation.

Comparison of the Cosmic-Ray Neutron Probe with the Distributed Sensor Network

To compare the CRNP areal soil moisture with the TDT in situ distributed sensor network measurements or with the numerically simulated soil moisture values, the point soil moisture measurements or simulations were computed with a horizontal and vertical averaging weight function given by (Franz et al., 2012)

$$\overline{\theta} = \sum \mathrm{wt}(z) \left[\sum_{i=1}^{n} \mathrm{wt}(r) \theta_i(z) \right] \quad [6]$$

where $\overline{\theta}$ is the average areal soil moisture measurement of the TDT network or the Hydrus-1D simulation for the TWDEF site, wt(z) is a linear depth-weighted factor at a depth of z, wt(r) is a horizontal weight factor at a distance r from the CRNP, $\theta_i(z)$ is the measured or simulated soil water content at a depth of z in the ith subplot, and n is the total number of subplots (i.e., n = 36).

The vertical weighting factor, wt(z), was shown to have good agreement with a nonlinear method (Hawdon et al., 2014) and was calculated using a linear depth-weighted function (Franz et al., 2012):

$$\mathrm{wt}(z) = \begin{cases} \alpha_z \left[1 - \dfrac{z}{z^*(\theta_v)} \right] & 0 \le z \le z^*(\theta_v) \\ 0 & z > z^*(\theta_v) \end{cases} \quad [7]$$

where α_z is a function in which the weights sum to unity, defined as

$$\int_0^{z^*(\theta_v)} \alpha_z \left[1 - \frac{z}{z^*(\theta_v)} \right] dz = 1 \quad [8]$$

yielding the solution $\alpha_z = 2/z^*(\theta_v)$.

Horizontal weighting was obtained from a relationship between the cumulative fraction of counts and the CRNP footprint radius (Zreda et al., 2008). This relationship is simplified as

$$\mathrm{wt}(r) = \begin{cases} \alpha_r \left(1 - \dfrac{r}{R} \right) & 0 \le r \le R \\ 0 & r > R \end{cases} \quad [9]$$

where α_r is a constant defined as before by the condition that the weights sum to unity:

$$\int_0^R \alpha_r \left(1 - \frac{r}{R} \right) dr = 1 \quad [10]$$

where R is the footprint radius of 385 m for the TWDEF site and α_r = 0.0052.

As noted, the TWDEF CRNP footprint is circular, with a radius of 385 m. Figure 1 illustrates how the TDT sensor network covers only part of the CRNP footprint. However, the contribution of neutron counts decreases rapidly with distance away from the CRNP (Zreda et al., 2008). The study of Bogena et al. (2013) calculated that approximately 54 and 80% of the cumulative fraction of neutron counts were contributed from distances of 100 and 200 m, respectively. At the TWDEF, the distal TDT sensors installed in aspen, conifer, grass, and sagebrush were approximately 185, 260, 201, and 140 m from the CRNP, respectively. We also compared the spatial average soil moisture calculated from the TDR field measurements with the in situ TDT measurements in the upper 0.1-m depth, with the differences determined to be <0.004 m^3/m^3. These results indicated a consistent spatial mean produced by both TDR and TDT. Therefore, the soil moisture computed from the TDT sensor network at the TWDEF site lies within a significant portion (60%) of the CRNP sensing footprint. Coopersmith et al. (2014) also reported reliable soil moisture estimates from a partial footprint of a CRNP.

Results and Discussion

We first compared the CRNP estimated soil moisture with the TDT soil moisture sensor network comprised of 36 locations with three sensor depths in each subplot. We then examined the improvement of the TDT sensor network results by introducing numerical simulations of near-surface soil moisture (0–0.1 m) using the Hydrus-1D program. To explore an observed bias between the CRNP-estimated soil moisture and the TDT-sensor-based areal averaged soil moisture, we evaluated the soil moisture characteristics surrounding the CRNP according to vegetation type and soil texture. These two characteristics exhibited significant heterogeneity and were correlated with soil moisture within the instrumented domain. We also analyzed seasonal changes in the soil moisture field, which were shown to have a significant effect on the horizontal heterogeneity of the CRNP output.

Soil Moisture Comparison of the Cosmic-Ray Neutron Probe with the Time-Domain Transmissometry Network

To compare soil moisture measurements from the TDT network (θ_{TDT}) with the estimated soil moisture (θ_v) from the CRNP using Eq. [4], we computed TDT weighted average areal soil moisture ($\overline{\theta}_{TDT}$) by assigning horizontal weight factors to each subplot and vertical weight factors to each sensor depth. The comparison is shown in Fig. 2a. The RSME and R^2 between $\overline{\theta}_{TDT}$ and θ_v were 0.011 m^3/m^3 and 0.74, respectively, in 2011 and 0.023 m^3/m^3 and 0.81, respectively, in 2012. The difference between $\overline{\theta}_{TDT}$ and θ_v

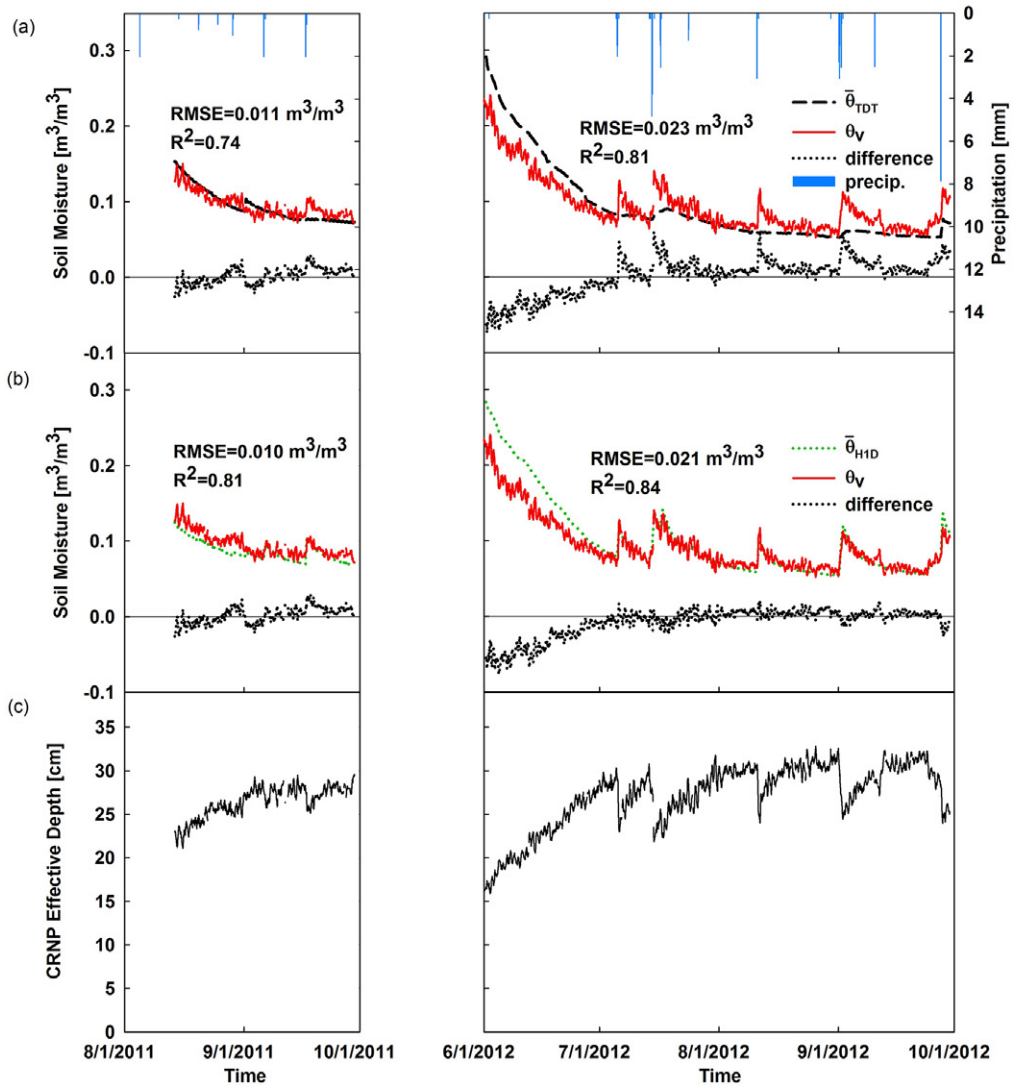

Fig. 2. (a) Comparison between time domain transmissometry (TDT) weighted hourly average soil moisture at 0.1-, 0.25-, and 0.5-m depths ($\overline{\theta}_{TDT}$) and the average areal soil moisture measured by cosmic-ray neutron probe (CRNP) (θ_v) during the growing seasons of 2011 and 2012; (b) comparison between Hydrus-1D weighted soil moisture ($\overline{\theta}_{H1D}$) at 0.03-, 0.05-, 0.1-, 0.25-, and 0.5-m depths and θ_v during the growing seasons of 2011 and 2012 (the soil moisture at 0.03 and 0.05 m was extracted from the Hydrus-1D estimation; the soil moisture at 0.1, 0.25, and 0.5 m was measured by TDT sensors); and (c) the effective depth $z^*(\theta_v)$, which was calculated using Eq. [5].

was as high as 0.08 m^3/m^3 during the growing season of 2012. The CRNP averaged areal soil moisture response was sensitive to small rainfall events in the late summer; however, due to the 0.1-m or deeper burial depth of the TDT soil moisture sensors, the TDT weighted soil moisture response was insensitive to rainfall events at the TWDEF site (Fig. 2a).

Franz et al. (2012) concluded that the CRNP is more sensitive to soil moisture at shallower depths (0–0.1 m) than deeper depths. To estimate soil moisture values in the near surface, we applied the Hydrus-1D numerical model to predict the van Genuchten soil hydraulic parameters in soil locations where TDT sensors were installed.

Figure 3 shows examples of simulated and observed soil moisture at the 0.1-, 0.25-, and 0.5-m depths and Hydrus-1D estimated soil moisture at the 0.03- and 0.05-m depths for the four vegetation types during the 2012 growing season. Simulated and observed water contents were well matched in most instances. Correlation between simulated and observed soil moisture at the 0.1-, 0.25-, and 0.5-m depths were >0.8, and the means of the correlation and RMSE were around 0.95 and 0.005 m^3/m^3, respectively, indicating a very good fit for model simulations. The optimized hydraulic properties (saturated water content θ_s, shape parameters α and n, and saturated hydraulic conductivity K_s) including their 95% confidence intervals were calculated using Hydrus-1D (H1D) for each simulation as shown in Fig. 4. The narrow confidence intervals were obtained from the inverse simulation of an aspen site (A1), and the highest uncertainty occurred when the soil was close to saturation.

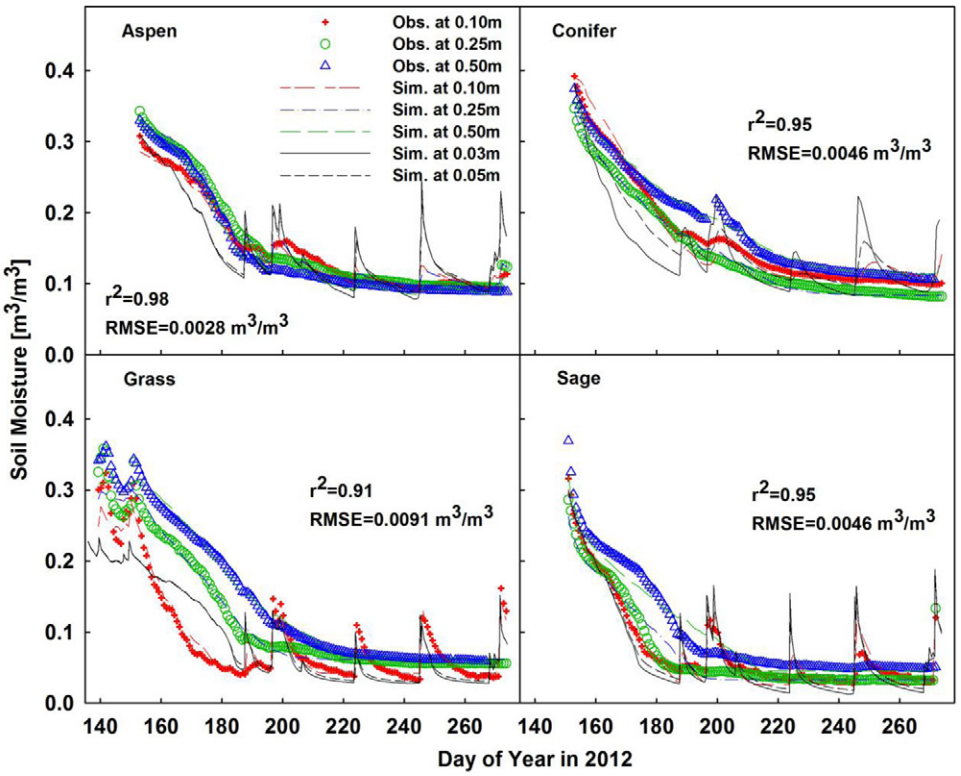

Fig. 3. Example of simulated (Sim.) vs. observed (Obs.) soil moisture values at 0.1-, 0.25-, and 0.5-m depths and simulated soil moisture at 0.03- and 0.05-m depths in aspen, conifer, grass, and sagebrush sites during the 2012 study period.

Table 4 illustrates a few examples of the soil hydraulic parameters estimated using inverse simulation with the numerical model. The large θ_s values derived from our optimization are consistent with forest soils containing burrowing animals (e.g., pocket gophers) coupled with the sustained high soil moisture values during snowmelt. Using these parameters, we extracted soil moisture estimates at the 0.03- and 0.05-m depths using forward numerical simulations. We then applied the simulated soil moisture values at 0.03 and 0.05 m combined with the TDT-measured soil moisture values at 0.1, 0.25, and 0.5 m to compute the areal-averaged weighted soil moisture ($\overline{\theta}_{H1D}$) using the same methods. Compared with $\overline{\theta}_{TDT}$, the $\overline{\theta}_{H1D}$ values showed marked improvement in soil moisture estimates during rainfall events (Fig. 2b). The absolute difference between θ_v and $\overline{\theta}_{H1D}$ was <0.02 m^3/m^3 when rainfall occurred. The RSME and R^2 between θ_v and $\overline{\theta}_{H1D}$ were 0.021 m^3/m^3 and 0.84. The considerable high differences between θ_v and $\overline{\theta}_{H1D}$ at the beginning of the growing season of 2012 still exist.

As we noted, both $\overline{\theta}_{TDT}$ and $\overline{\theta}_{H1D}$ agreed well with θ_v during relatively dry periods. The RMSE was 0.009 m^3/m^3 and R^2 was 0.96 when θ_v was $\leq$0.1 m^3/m^3. For θ_v >0.1 m^3/m^3, the CRNP estimate of soil moisture underpredicted the independently determined methods. One possible explanation for this discrepancy may be a result of the timing and soil moisture distribution during the field calibration of the CRNP, yielding the constants used in Eq. [4] (i.e., $a_0 = 0.0808$, $a_1 = 0.372$, and $a_2 = 0.115$). We therefore felt it was necessary to re-examine the calibration and soil moisture impacting the CRNP at the TWDEF site.

Vegetation Related Soil Moisture Distribution within the Experimental Forest Site

As stated above, the TWDEF site is a patchwork of four dominant vegetation types. The CRNP was installed near the center of the meadow, which is surrounded by trees. To explore the spatial organization of soil moisture at the TWDEF site resulting from the vegetation structure, soil moisture

was measured between the 0- and 0.1-m depths using the portable TDR. The results were divided into four groups based on the dominant vegetation coverage in a given area.

The seasonal evolution of the soil moisture for each vegetation type is shown in Fig. 5. During the wet period (7 June), the mean and standard deviation (SD) of soil moisture for each vegetation type were 0.225 ± 0.045, 0.245 ± 0.062, 0.14 ± 0.052, and 0.15 ± 0.050 m^3/m^3 for aspen, conifer, grass, and sagebrush, respectively. Through processes of evapotranspiration and deep drainage, the soil moisture gradually decreased to a minimum value. In the dry period (1 August), the mean and SD of soil moisture were 0.050 ± 0.006, 0.052 ± 0.007, 0.047 ± 0.008, and 0.044 ± 0.007 m^3/m^3 for aspen, conifer, grass, and sagebrush, respectively. Mean soil moisture values underneath tree canopies were significantly higher ($P < 0.005$) than values under grass and sagebrush. One possible reason for this is the dominance of the soil clay content associated with trees compared with grass and sagebrush (Fig. 6). The relationship between clay content and soil moisture is illustrated in Fig. 7. We also looked at the relationship between TDT sensor installation locations and soil clay content, where clay content was grouped into three categories: high clay content (>17%), medium clay content (10–17%), and low clay content (<10%). As expected,

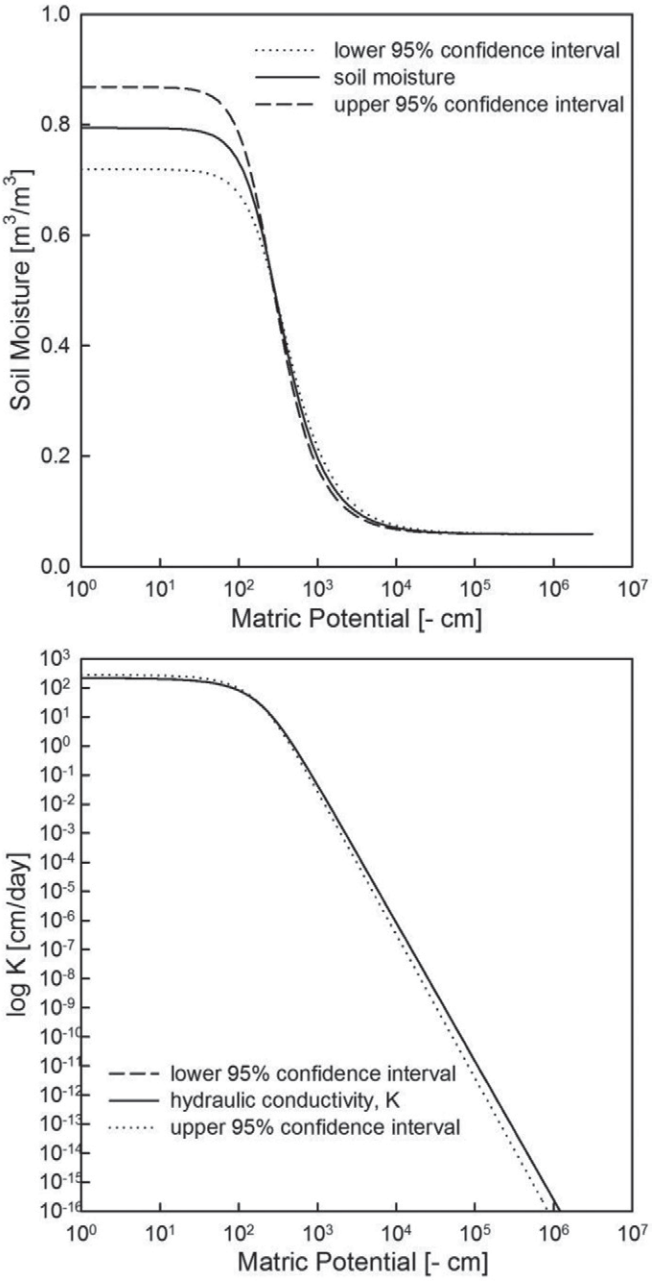

Fig. 4. Example of simulated hydraulic properties and corresponding 95% confidence intervals for (a) soil moisture and (b) hydraulic conductivity (K) for the top layer of AA1, which is Subplot 1 of Plot A under aspen

Table 4. Numerically fit (Hydrus-1D) soil hydraulic parameters including the residual and saturated water contents (θ_r and θ_s, respectively), shape factors a and n, and saturated hydraulic conductivity (K_s), from one of nine possible subplots (A1, A2, A3, B1, B2, ...) for each vegetation type.

Vegetation	Depth	θ_r	θ_s	α	n	K_s
	m	—— m^3/m^3 ——		1/m		m/d
Aspen A1	0.10	0.059	0.794	0.444	2.106	2.159
	0.25	0.059	0.444	0.214	1.901	0.086
	0.5	0.04	0.490	0.228	1.632	0.046
Conifer A1	0.10	0.045	0.442	0.338	1.333	0.121
	0.25	0.051	0.430	0.231	1.408	0.477
	0.5	0.044	0.428	0.099	1.642	0.014
Grass A1	0.10	0.01	0.400	0.943	1.402	0.460
	0.25	0.053	0.600	0.441	1.761	0.012
	0.5	0.066	0.636	0.357	2.207	0.563
Sagebrush A1	0.10	0.015	0.513	0.966	1.665	1.113
	0.25	0.018	0.629	2.420	1.556	4.797
	0.5	0.045	0.68	0.4053	2.704	1.430

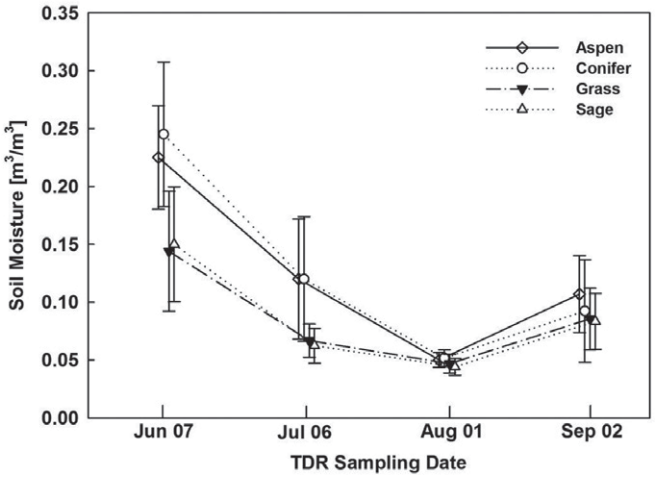

Fig. 5. The seasonal evolution of soil moisture under the four vegetation types as measured by the portable time domain reflectometry (TDR) probe on 7 June 2012, 6 July 2012, 1 Aug. 2012, and 2 Sept. 2012 at the T.W. Daniel Experimental Forest site. The error bars represent ±1 SD.

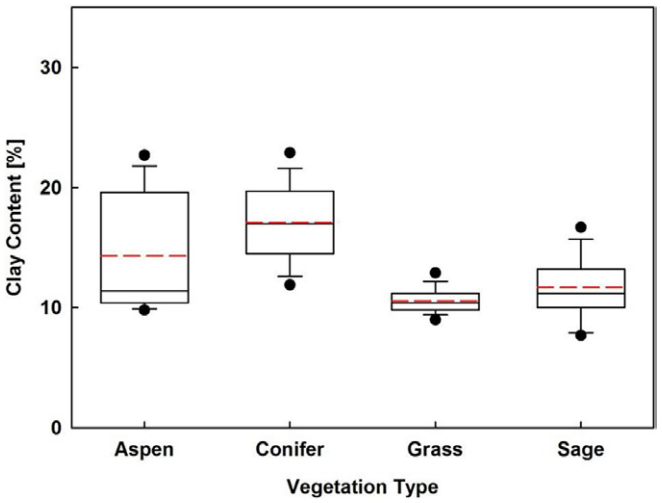

Fig. 6. Clay content distribution within each vegetation type based on electromagnetic induction mapping and correlation between clay content and apparent electrical conductivity (EC_a). From top to bottom, the box chart shows the maximum value (top whisker), 75th percentile, mean (dashed line), median (solid line), 25th percentile, and minimum value (bottom whisker) for the respective vegetation group. Dots indicate the 95th and 5th confidence intervals.

for a given sampling date, locations with higher clay content exhibited higher soil water content. Soil moisture at locations with clay contents >17% showed significantly higher ($P < 0.05$) soil moisture than the other two groups over time.

Seasonal Change of Soil Moisture Distribution

We used variograms of the soil moisture distribution measured using a portable TDR to characterize the seasonal change in soil moisture in the TWDEF research site. The nugget, sill, range, and nugget/sill ratio (nugget contribution) are listed in Table 5. The range in June was >100 m. The apparent range decreased in July and was virtually gone in August. In other words, soil moisture exhibited strong spatial structure in early summer when the soil profile was wet, but that structure became random by August, in agreement with observations of soil moisture patterns made by others (Western and Grayson, 1998). Rainfall in September brought back the spatial structure of soil moisture, which had a longer range but was more random than August soil moisture because the nugget contribution was higher.

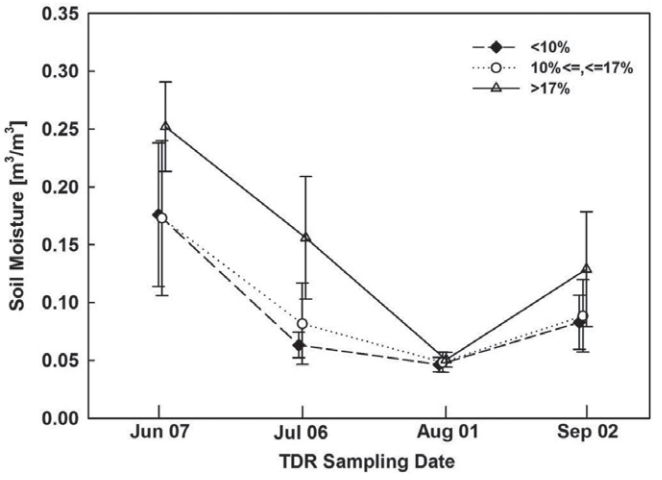

Fig. 7. Temporal evolution of soil moisture during the summer of 2012 within each of three soil clay content regimes illustrated in Fig. 1. The mean soil moisture flanked by one standard deviation for each soil clay fraction are plotted from portable time domain reflectometry measurements made on 7 June 2012, 6 July 2012, 1 Aug. 2012, and 2 Sept. 2012 at the T.W. Daniel Experimental Forest.

The soil textural distribution together with the similar vegetation distribution illustrated in Fig. 1 generates a dry–wet strip-like spatial soil moisture distribution surrounding the CRNP, which is strongly exhibited after snowmelt (see Fig. 5). This soil moisture distribution evolves from this binary distribution toward a Gaussian distribution as the soil dries down. With the initial calibration being performed under dry conditions, the binary distribution under wet conditions probably caused underestimation of the soil moisture by the CRNP. This underestimation was more pronounced during the beginning of the growing season and was minimized as the soil dried (Franz et al., 2013).

Effect of Vegetation Biomass on the Calibration

The CRNP is sensitive to all H sources and, as such, requires accounting for and calibration of these sources. In calibrating the CRNP, we have accounted for atmospheric water vapor, soil organic matter, and lattice water but lack a correction for vegetation biomass at the TWDEF. The presence of vegetation will affect the neutron counting rates, which further leads to bias in the soil moisture estimates of the CRNP.

The trees, on the other hand, exhibit both ongoing tree ring increment as well as seasonal growth of leaves and stems. The growth and loss of aspen leaves, for example, accounts for around 3 to 5% of the total aboveground biomass (Johnston and Bartos, 1977; West and Reese, 1991). The sagebrush is also somewhat constant, while the grasses and forbs are highly seasonal, exhibiting peak presence in the late spring and summer. While the vegetation

Table 5. Variogram nugget and sill from soil moisture measurements for each of four different sampling dates in 2012. The variogram was fitted to the soil water content measurements obtained from a portable time domain reflectometry probe using an exponential model.

Date	Mean	Nugget	Sill	Range	R^2	Nugget contribution
	m^3/m^3	—— m^6/m^6 ——		m		
June 7	0.175	0.001023	0.01053	137	0.92	0.09
July 6	0.088	0.000105	0.00243	90	0.91	0.04
Aug. 1	0.046	0.000171	0.00033	–	–	0.34
Sept. 2	0.094	0.001330	0.00068	195	0.93	0.66

impact on the CRNP reading is certainly of interest, our instrumented area was determined to be insufficiently representative both in terms of its size and vegetation distribution relative to those of the CRNP footprint. We therefore have assumed that vegetation impacts are accounted for in the original and any subsequent CRNP calibrations.

The calibration procedure enables us to derive a site-specific calibration parameter, N_0, which includes the effects of biomass. It has been shown that N_0 remains constant with time unless there is significant vegetation change throughout the year (Bogena et al., 2013; Chrisman and Zreda, 2013; Hawdon et al., 2014). We have assumed that the TWDEF has experienced minimal biomass change during a 2- to 3-yr period, and therefore biomass was accounted for in the calibration.

Recalibration of Cosmic-Ray Neutron Probe for the Experimental Forest site

For specific site conditions, it is critical to establish local CRNP calibration functions. We attempted to re-fit the parameters in Eq. [4] (a_0, a_1, and a_2) to improve the CRNP estimates for our site, given our measured and modeled seasonal soil moisture. Using the solver in Excel, an objective function was established to minimize the sum of squared errors between the CRNP values and the numerical simulated values including the important near-surface estimates. The RMSE and R^2 for this optimization were 0.012 m^3/m^3 and 0.95 between $\overline{\theta}_{H1D}$ during 2012 and the soil moisture, θ_v', computed from the recalibrated parameters of Eq. [4] with a_0 = 0.012, a_1 = 0.367, and a_2 = 0.227.

Compared with the parameters of Desilets et al. (2010), the newly fitted parameters yielded soil moisture estimates which were much better correlated with the Hydrus-1D weighted average areal soil moisture as shown in Fig. 8. To evaluate our recalibration, we calculated θ_v and $\overline{\theta}_{TDT}$ for the growing season in 2013 using the same procedures as in 2011 and 2012 and compared them with θ_v' during the same period of 2013 (Fig. 9). In 2013, before recalibration, the RMSE and R^2 between θ_v and $\overline{\theta}_{TDT}$ were 0.025 m^3/m^3 and 0.87, respectively. After recalibration, the RMSE and R^2 were 0.011 m^3/m^3 and 0.97, respectively. The results demonstrate the improved CRNP correlation with the measured soil moisture values, especially during the wet season, with an R^2 value between θ_v' and $\overline{\theta}_{TDT}$ of 0.95. This result strengthens the idea that a single-day calibration for the CRNP, which has been a standard practice performed during installation, may be inadequate for accurate soil moisture determination. We found that the seasonally varying soil moisture distribution modes surrounding the CRNP necessitated additional calibration effort, especially during the wet season. The extra effort included independently checking seasonal soil moisture values within the CRNP footprint, which for us included a TDT-based soil moisture network, numerical modeling of the near surface, and manual measurements of soil moisture in the upper 0.1 m of soil.

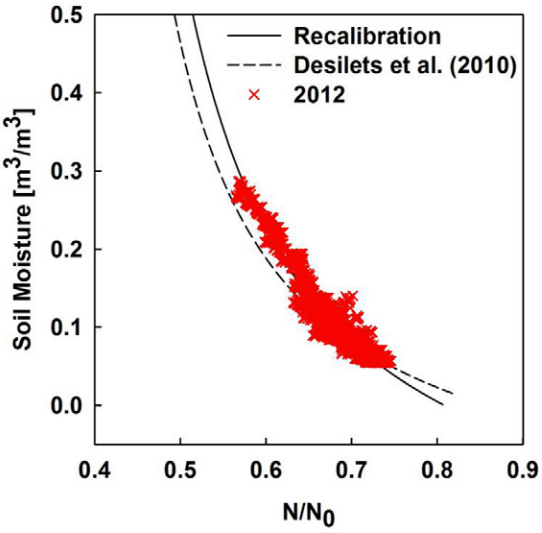

Fig. 8. Comparison of cosmic-ray neutron probe (CRNP)-based soil moisture estimates as a function of fast neutron intensity using the parameters of Desilets et al. (2010) against recalibrated parameters for the T.W. Daniel Experimental Forest. The discrete data points are derived from the Hydrus-1D weighted average areal soil moisture ($\overline{\theta}_{H1D}$) and the relative fast neutron intensity (N/N_0) obtained during the growing season of 2012.

Conclusions

In this study, we compared the CRNP soil moisture measurements and in situ distributed TDT sensor soil moisture network measurements. Lacking TDT water content measurements in the near surface (>0.1 m), we used numerical simulations of soil moisture to provide estimates of shallow soil moisture. We evaluated the relationship between soil moisture distribution patterns and soil texture as well as vegetation structure within the study site. We found soil moisture underneath trees to be significantly higher than soil moisture beneath grass or sagebrush, which showed correlation with soil texture as well. The differences between tree

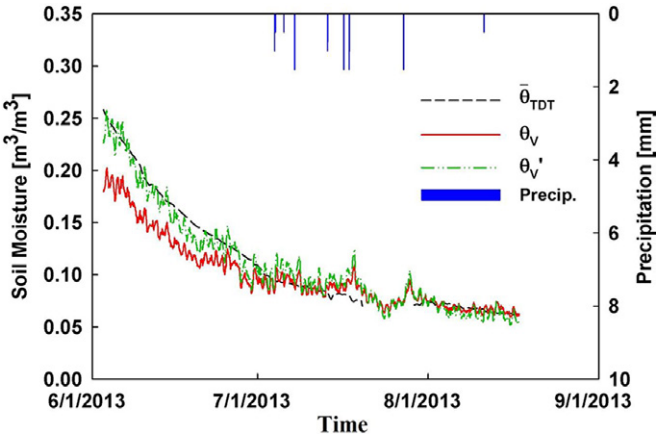

Fig. 9. Comparison of soil moisture estimated from the weighted time domain transmissometry (TDT) sensors ($\overline{\theta}_{H1D}$), the universal calibration function (θ_v), and the recalibrated parameters (θ_v') during the snow-free season of 2013.

soil moisture and soil moisture under grass or sagebrush was substantial under wet conditions but vanished under dry conditions. The CRNP location in the central portion of the meadow at the TWDEF site turned out to be a relatively dry location (i.e., coarse-textured, sandy soil). We used manual sampling of soil moisture to characterize the seasonal change in the soil moisture distribution with time, revealing a nearly binary distribution early in the growing season when the soil was wet and a shift toward reduced structure and a Gaussian soil moisture distribution as the soil dried out. This led to our observation that the original CRNP calibration yielded an underestimate of soil moisture under wet conditions. A recalibrated CRNP function between neutron count and a combination of soil moisture measurements and near-surface simulations was established by fitting the parameters $a_0 = 0.120$, $a_1 = 0.367$, and $a_2 = 0.227$. Compared with the RMSE and R^2 between $\overline{\theta}_{TDT}$ and θ_v in 2013, the recalibration reduced the RMSE from 0.025 to 0.011 m^3/m^3 and increased R^2 from 0.8 to 0.97. Our study implies that multiple calibrations could improve the determination of the parameters involved in the calibration function; we therefore recommend more than one calibration for COSMOS systems. However, the timing distribution of each calibration was according to the change in soil moisture characteristics in a specific CRNP site.

Acknowledgments

This research was supported by a National Science Foundation (NSF) EPSCoR Grant EPS 1208732 awarded to Utah State University, as part of the State of Utah Research Infrastructure Improvement Award. Additional support was provided by a project of USDA-CSREES Special Research Grant no. 2008-34552-19042 from the USDA Cooperative State Research, Education, and Extension Service and by the Utah Agricultural Experiment Station, Utah State University, Logan, approved as Journal Paper no. 8724. Furthermore, we express appreciation to the Chinese Scholarship Council (CSC) and to the School of Graduate Studies at Utah State University for student financial support. We express sincere appreciation to Hiruy Abdu for EMI mapping of the site and to Jobie Carlisle for outstanding instrumentation management and technical support at the TWDEF. Any opinions, findings, and conclusions or recommendations expressed are those of the author(s) and do not necessarily reflect the views of the NSF or USDA.

References

Abdu, H., D.A. Robinson, M. Seyfried, and S.B. Jones. 2008. Geophysical imaging of watershed subsurface patterns and prediction of soil texture and water holding capacity. Water Resour. Res. 44:W00D18. doi:10.1029/2008WR007043

Blonquist, J.M., Jr., S.B. Jones, and D.A. Robinson. 2005a. Standardizing characterization of electromagnetic water content sensors: 2. Evaluation of seven sensing systems. Vadose Zone J. 4:1059–1069. doi:10.2136/vzj2004.0141

Blonquist, J.M., Jr., S.B. Jones, and D.A. Robinson. 2005b. A time domain transmission sensor with TDR performance characteristics. J. Hydrol. 314:235–245. doi:10.1016/j.jhydrol.2005.04.005

Boettinger, J.L., J.R. Lawley, and H. Van Miegroet. 2004. Morphology of soils in the aspen, conifer, grass/forbs, and sagebrush environmental monitoring sites. TW Daniel Exp. For., Logan, UT. http://twdef.usu.edu/view.html

Bogena, H.R., J.A. Huisman, R. Baatz, H.J.H. Franssen, and H. Vereecken. 2013. Accuracy of the cosmic-ray soil water content probe in humid forest ecosystems: The worst case scenario. Water Resour. Res. 49:5778–5791. doi:10.1002/wrcr.20463

Bogena, H.R., J.A. Huisman, C. Oberdörster, and H. Vereecken. 2007. Evaluation of a low-cost soil water content sensor for wireless network applications. J. Hydrol. 344:32–42. doi:10.1016/j.jhydrol.2007.06.032

Chrisman, B., and M. Zreda. 2013. Quantifying mesoscale soil moisture with the cosmic-ray rover. Hydrol. Earth Syst. Sci. 17:5097–5108. doi:10.5194/hess-17-5097-2013

Coopersmith, E.J., M.H. Cosh and C.S.T. Daughtry. 2014. Field-scale moisture estimates using COSMOS sensors: A validation study with temporary networks and leaf-area-indices. J. Hydrol. 519:637–643. doi:10.1016/j.jhydrol.2014.07.060

Crow, W.T., A.A. Berg, M.H. Cosh, A. Loew, B.P. Mohanty, R. Panciera, et al. 2012. Upscaling sparse ground-based soil moisture observations for the validation of coarse-resolution satellite soil moisture products. Rev. Geophys. 50:RG2002. doi:10.1029/2011RG000372

Desilets, D., and M. Zreda. 2013. Footprint diameter for a cosmic-ray soil moisture probe: Theory and Monte Carlo simulations. Water Resour. Res. 49:3566–3575. doi:10.1002/wrcr.20187

Desilets, D., M. Zreda, and T.P.A. Ferré. 2010. Nature's neutron probe: Land surface hydrology at an elusive scale with cosmic rays. Water Resour. Res. 46:W11505. doi:10.1029/2009WR008726

Feddes, R.A., E. Brester, and S.P. Neuman. 1974. Field test of a modified numerical model for water uptake by root systems. Water Resour. Res. 10:1199–1206. doi:10.1029/WR010i006p01199

Feddes, R.A., H. Hoff, M. Bruen, T. Dawson, P. de Rosnay, D. Paul, et al. 2001. Modeling root water uptake in hydrological and climate models. Bull. Am. Meteorol. Soc. 82:2797–2809. doi:10.1175/1520-0477(2001)082<2797:MRWUIH>2.3.CO;2

Flinn, K.M., and P.L. Marks. 2007. Agricultural legacies in forest environments: Tree communities, soil properties, and light availability. Ecol. Appl. 17:452–463. doi:10.1890/05-1963

Franz, T.E., M. Zreda, T.P.A. Ferre, and R. Rosolem. 2013. An assessment of the effect of horizontal soil moisture heterogeneity on the area-average measurement of cosmic-ray neutrons. Water Resour. Res. 49:6450–6458. doi:10.1002/wrcr.20530

Franz, T.E., M. Zreda, R. Rosolem, and T.P.A. Ferre. 2012. Field validation of a cosmic-ray neutron sensor using a distributed sensor network. Vadose Zone J. 11(4). doi:10.2136/vzj2012.0046

Friedman, S.P. 2005. Soil properties influencing apparent electrical conductivity: A review. Comput. Electron. Agric. 46:45–70. doi:10.1016/j.compag.2004.11.001

Havranek, W., and U. Benecke. 1978. The influence of soil moisture on water potential, transpiration and photosynthesis of conifer seedlings. Plant Soil 49:91–103. doi:10.1007/BF02149911

Hawdon, A., D. McJannet, and J. Wallace. 2014. Calibration and correction procedures for cosmic-ray neutron soil moisture probes located across Australia. Water Resour. Res. 50:5029–5043. doi:10.1002/2013WR015138

Hawley, M.E., T.J. Jackson, and R.H. McCuen. 1983. Surface soil moisture variation on small agricultural watersheds. J. Hydrol. 62:179–200. doi:10.1016/0022-1694(83)90102-6

Jenkins, J.C., D.C. Chojnacky, L.S. Heath, and R.A. Birdsey. 2003. National-scale biomass estimators for United States tree species. For. Sci. 49:12–35.

Johnston, R.S. and D.L. Bartos. 1977. Summary of nutrient and biomass data from two aspen sites in western United States. Res. Note INT-227. U.S. For. Serv., Intermt. For. Range Exp. Stn., Ogden, UT.

Jones, S.B., J.M. Blonquist, D.A. Robinson, V.P. Rasmussen, and D. Or. 2005. Standardizing characterization of electromagnetic water content sensors. Vadose Zone J. 4:1048–1058. doi:10.2136/vzj2004.0140

Kelliher, F.M., R. Leuning, and E.D. Schulze. 1993. Evaporation and canopy characteristics of coniferous forests and grasslands. Oecologia 95:153–163. doi:10.1007/BF00323485

Kolb, K.J., and J.S. Sperry. 1999. Transport constraints on water use by the Great Basin shrub, *Artemisia tridentata*. Plant Cell Environ. 22:925–935. doi:10.1046/j.1365-3040.1999.00458.x

Kramer, J.H., S.J. Cullen, and L.G. Everett. 1992. Vadose zone monitoring with the neutron moisture probe. Ground Water Monit. Rem. 12:177–187. doi:10.1111/j.1745-6592.1992.tb00058.x

Lesch, S.M., J.D. Rhoades, and D.L. Corwin. 2000. The ESAP-95 version 2.01R user manual and tutorial guide. USDA–ARS, U.S. Salinity Lab., Riverside, CA.

Lesch, S.M., D.J. Strauss, and J.D. Rhoades. 1995. Spatial prediction of soil salinity using electromagnetic induction techniques: 2. An efficient spatial sampling algorithm suitable for multiple linear regression model identification and estimation. Water Resour. Res. 31:387–398. doi:10.1029/94WR02180

McArthur, E.D. 1983. Taxonomy, origin, and distribution of big sagebrush (*Artemisia tridentata*) and allies (subgenus *Tridentatae*). In: K.L. Johnson, editor, Proceedings of the First Utah Shrub Ecology Workshop, Ephraim, UT. 9–10 Sept. 1981. Utah State Univ., Logan. p. 3–13.

McJannet, D., T. Franz, A. Hawdon, D. Boadle, B. Baker, A. Almeida, et al. 2014. Field testing of the universal calibration function for deter-

mination of soil moisture with cosmic-ray neutrons. Water Resour. Res. 50:5235–5248. doi:10.1002/2014WR015513

Minet, J., E. Laloy, S. Lambot, and M. Vanclooster. 2011. Effect of high-resolution spatial soil moisture variability on simulated runoff response using a distributed hydrologic model. Hydrol. Earth Syst. Sci. 15:1323–1338. doi:10.5194/hess-15-1323-2011

Ochsner, T.E., M.H. Cosh, R.H. Cuenca, W.A. Dorigo, C.S. Draper, Y. Hagimoto, et al. 2013. State of the art in large-scale soil moisture monitoring. Soil Sci. Soc. Am. J. 77:1888–1919. doi:10.2136/sssaj2013.03.0093

Olsen, H.R., and H. Van Miegroet. 2010. Factors affecting carbon dioxide release from forest and rangeland soils in northern Utah. Soil Sci. Soc. Am. J. 74:282–291. doi:10.2136/sssaj2009.0095

Reynolds, S.G. 1970. The gravimetric method of soil moisture determination: III. An examination of factors influencing soil moisture variability. J. Hydrol. 11:288–300. doi:10.1016/0022-1694(70)90068-5

Robinson, D.A., C.S. Campbell, J.W. Hopmans, B.K. Hornbuckle, S.B. Jones, R. Knight, et al. 2008. Soil moisture measurement for ecological and hydrological watershed-scale observatories: A review. Vadose Zone J. 7:358–389. doi:10.2136/vzj2007.0143

Robinson, D.A., S.B. Jones, J.M. Wraith, D. Or, and S.P. Friedman. 2003a. A review of advances in dielectric and electrical conductivity measurement in soils using time domain reflectometry. Vadose Zone J. 2:444–475. doi:10.2136/vzj2003.4440

Robinson, D.A., M. Schaap, S.B. Jones, S.P. Friedman, and M.K. Gardner. 2003b. Considerations for improving the accuracy of permittivity measurement using TDR: Air–water calibration, effects of cable length. Soil Sci. Soc. Am. J. 67:62–70. doi:10.2136/sssaj2003.6200

Rosenbaum, U., J.A. Huisman, A. Weuthen, H. Vereecken, and H.R. Bogena. 2010. Sensor-to-sensor variability of the ECH_2O EC-5, TE, and 5TE sensors in dielectric liquids. Vadose Zone J. 9:181–186. doi:10.2136/vzj2009.0036

Rosolem, R., W.J. Shuttleworth, M. Zreda, T.E. Franz, X. Zeng, and S.A. Kurc. 2013. The effect of atmospheric water vapor on neutron count in the Cosmic-Ray Soil Moisture Observing System. J. Hydrometeorol. 14:1659–1671. doi:10.1175/JHM-D-12-0120.1

Running, S.W. 1976. Environmental control of leaf water conductance in conifers. Can. J. For. Res. 6:104–112. doi:10.1139/x76-013

Ryel, R., M. Caldwell, C. Yoder, D. Or, and A. Leffler. 2002. Hydraulic redistribution in a stand of *Artemisia tridentata*: Evaluation of benefits to transpiration assessed with a simulation model. Oecologia 130:173–184. doi:10.1007/s004420100794

Ryel, R.J., A.J. Leffler, C. Ivans, M.S. Peek, and M.M. Caldwell. 2010. Functional differences in water-use patterns of contrasting life forms in Great Basin steppelands. Vadose Zone J. 9:548–560. doi:10.2136/vzj2010.0022

Schwartz, R.C., J.J. Casanova, J.M. Bell, and S.R. Evett. 2014. A reevaluation of time domain reflectometry propagation time determination in soils. Vadose Zone J. 13(1). doi:10.2136/vzj2013.07.0135

Scipal, K., C. Scheffler, and W. Wagner. 2005. Soil moisture–runoff relation at the catchment scale as observed with coarse resolution microwave remote sensing. Hydrol. Earth Syst. Sci. Discuss. 2:417–448. doi:10.5194/hessd-2-417-2005

Seneviratne, S.I., T. Corti, E.L. Davin, M. Hirschi, E.B. Jaeger, I. Lehner, et al. 2010. Investigating soil moisture–climate interactions in a changing climate: A review. Earth Sci. Rev. 99:125–161. doi:10.1016/j.earscirev.2010.02.004

Shuttleworth, W.J., M. Zreda, X. Zeng, C. Zweck, and T.P.A. Ferré. 2010. The Cosmic-ray Soil Moisture Observing System (COSMOS): A non-invasive, intermediate-scale soil moisture measurement network. In: C. Kirby, editor, Role of Hydrology in Managing Consequences of a Changing Global Environment: Proceedings of the BHS 3rd International Symposium, Newcastle, UK. 19–23 July 2010. Br. Hydrol. Soc., London.

Šimůnek, J., M. Sejna, H. Saito, M. Sakai, and M.Th. van Genuchten. 2008. The Hydrus-1D software package for simulating the movement of water, heat, and multiple solutes in variably saturated media. Version 4.0, HYDRUS Software Ser. 3. Dep. of Environ. Sci., Univ. of California, Riverside.

Taylor, S.T., and G.L. Ashcroft. 1972. Physical edaphology: The physics of irrigated and nonirrigated soils. W.H. Freeman & Co, San Francisco.

Topp, G.C., J.L. Davis, and A.P. Annan. 1980. Electromagnetic determination of soil water content: Measurements in coaxial transmission lines. Water Resour. Res. 16:574–582. doi:10.1029/WR016i003p00574

Topp, G.C., D.R. Lapen, G.D. Young, and M. Edwards. 2001. Evaluation of shaft-mounted TDT readings in disturbed and undisturbed media. In: C.H. Dowding, editor, TDR 2001: 2nd International Symposium and Workshop on Time Domain Reflectometry for Innovative Geotechnical Applications, Evanston, IL. 5–7 Sept. 2001. Infrastruct. Technol. Inst., Evanston, IL.

Van Miegroet, H., J.L. Boettinger, M.A. Baker, J. Nielsen, D. Evans, and A. Stum. 2005. Soil carbon distribution and quality in a montane rangeland–forest mosaic in northern Utah. For. Ecol. Manage. 220:284–299. doi:10.1016/j.foreco.2005.08.017

Vereecken, H., J.A. Huisman, H. Bogena, J. Vanderborght, J.A. Vrugt, and J.W. Hopmans. 2008. On the value of soil moisture measurements in vadose zone hydrology: A review. Water Resour. Res. 44:W00D06. doi:10.1029/2008wr006829

Wang, K., P. Wang, J. Liu, M. Sparrow, S. Haginoya, and X. Zhou. 2005. Variation of surface albedo and soil thermal parameters with soil moisture content at a semi-desert site on the western Tibetan Plateau. Boundary-Layer Meteorol. 116:117–129. doi:10.1007/s10546-004-7403-z

West, N.E., and G.A. Reese. 1991. Comparison of some methods for collecting and analyzing data on aboveground net production and diversity of herbaceous vegetation in a northern Utah subalpine context. Vegetatio 96:145–163. doi:10.1007/BF00044976

Western, A.W., and R.B. Grayson. 1998. The Tarrawarra data set: Soil moisture patterns, soil characteristics, and hydrological flux measurements. Water Resour. Res. 34:2765–2768. doi:10.1029/98WR01833

Woldeselassie, M., H. Van Miegroet, M.-C. Gruselle, and N. Hambly. 2012. Storage and stability of soil organic carbon in aspen and conifer forest soils of northern Utah. Soil Sci. Soc. Am. J. 76:2230–2240. doi:10.2136/sssaj2011.0364

Yu, Z., H. Lü, Y. Zhu, S. Drake, and C. Liang. 2010. Long-term effects of revegetation on soil hydrological processes in vegetation-stabilized desert ecosystems. Hydrol. Processes 24:87–95. doi:10.1002/hyp.7472

Zreda, M., D. Desilets, T.P.A. Ferré, and R.L. Scott. 2008. Measuring soil moisture content non-invasively at intermediate spatial scale using cosmic-ray neutrons. Geophys. Res. Lett. 35:L21402. doi:10.1029/2008GL035655

Zreda, M., W.J. Shuttleworth, X. Zeng, C. Zweck, D. Desilets, T. Franz, et al. 2012. COSMOS: The COsmic-ray Soil Moisture Observing System. Hydrol. Earth Syst. Sci. Discuss. 9:4505–4551. doi:10.5194/hessd-9-4505-2012

Zreda, M., X. Zeng, W.J. Shuttleworth, C. Zweck, T.P.A. Ferre, T.E. Franz, and R. Rosolem. 2011. Cosmic-ray neutrons: An innovative method for measuring area-average soil moisture. GEWEX News 21:6–10.